


## Article

# Mechanical and Microstructural Features of Plasma Cut Edges in a 15 mm Thick S460M Steel Plate

Javier Aldazabal <sup>1,\*</sup> , Antonio Martín-Meizoso <sup>1</sup>, Andrzej Klimpel <sup>2</sup>, Adam Bannister <sup>3</sup> and Sergio Cicero <sup>4</sup>

<sup>1</sup> CEIT and Tecnun, University of Navarra, Manuel de Lardizábal 15, 20018 San Sebastián, Spain; ameizoso@ceit.es

<sup>2</sup> Politechnika Śląska—Sutil, ul. Komarskiego 18a, 44-100 Gliwice, Poland; andrzej.klimpel@polsl.pl

<sup>3</sup> Tata Steel, Swinden Technology Centre, Moorgate, Rotherham S60 3AR, UK; adam.bannister@tatasteel.com

<sup>4</sup> LADICIM (Laboratory of Materials Science and Engineering), E.T.S. de Ingenieros de Caminos, Canales y Puertos, University of Cantabria, Av/Los Castros 44, 39005 Santander, Spain; sergio.cicero@unican.es

\* Correspondence: jaldazabal@tecnun.es; Tel.: +34-943-219-877

Received: 4 May 2018; Accepted: 8 June 2018; Published: 11 June 2018



**Abstract:** In general, the thermal cutting processes of steel plates are considered to have an influence on microstructures and residual stress distribution, which determines the mechanical properties and performance of cut edges. They also affect the quality of the surface cut edges, which further complicates the problem, because in most cases the surface is subjected to the largest stresses. This paper studies the influence of plasma cutting processes on the mechanical behavior of the cut edges of steel and presents the characterization results of straight plasma arc cut edges of steel plate grade S460M, 15 mm thick. The cutting conditions used are the standard ones for industrial plasma cutting. The metallography of CHAZ (Cut Heat Affected Zones) and hardness profiles versus distance from plasma cut edge surface are tested; the mechanical behavior of different CHAZ layers under the cut edge surface were obtained by testing of instrumented mini-tensile 300  $\mu\text{m}$  thick specimens. Also, the residual stress distribution in the CHAZ was measured by X-ray diffraction. The results for the mechanical properties, microstructure, hardness, and residual stresses are finally compared and discussed. This work concludes that the CHAZ resulting from the plasma cutting process is narrow (about 700  $\mu\text{m}$ ) and homogeneous in plate thickness.

**Keywords:** plasma cutting; cut heat affected zone; mini-tensile test; steel plate; residual stress

## 1. Introduction

The use of steel plates in construction elements, structures, parts of machinery, etc. requires, in practically all cases, the cutting of these metallic sheets into smaller parts. These parts will later be connected to other elements using mechanical joints or welds. Nowadays we have at our disposal a plethora of cutting techniques: shear, oxy-cut, laser, plasma, water jet (with or without abrasive particles), thermal lance, etc., but all these cutting techniques introduce modifications in the regions close to the cut surface: they modify their surface roughness and, when they provide enough heat, they introduce modifications in the microstructure [1]. These changes result in local variations in the mechanical properties; in many cases, they also introduce or modify the profiles of the residual stresses in the areas close to the cutting surface [2–5]. A question arises here as to whether it is preferable to leave the cutting edge as it is or, on the contrary, if it is preferable to eliminate it, for example, by grinding (as specified or recommended in some construction standards [6,7]) to optimize the use of

the cut pieces and, in particular, their subsequent performance in applications under alternating loads (fatigue) [8–11].

Criteria to establish whether it is better to keep the original edge or to remove it was one of the objectives proposed within the European project HIPERCUT (“High Performance Cut Edges in Structural Steel Plates for Demanding Applications”, RSFR-CT-2012-00027 [12]). In this project, the results obtained using different cutting techniques were analyzed. Steel plates with thicknesses ranging from 8 mm up to 25 mm were studied, while the grades and mechanical strength of the plates varied between S355M and S890Q [13–16]. The cutting techniques that were analyzed and compared were plasma jet, laser beam, and oxyfuel (oxy-acetylene). This article presents the results obtained with the plasma cutting technique in a 15 mm S460M structural steel plate.

## 2. Materials and Methods

The characterization of the cutting edge obtained in a 15 mm thick steel plate with nominal yield stress of 460 MPa is summarized. The chemical composition of the steel was as follows (wt. %): 0.12 C, 0.45 Si, 1.49 Mn, 0.012 P, 0.001 S, 0.062 Cr, 0.001 Mo, 0.016 Ni, 0.048 Al, 0.011 Cu, 0.036 Nb, 0.005 N, 0.002 Sn, 0.003 Ti, 0.066 V. This plate was cut with a plasma jet, in the standard industrial conditions for the cutting of this thickness. The cutting parameters for the cutting equipment used (Hypertherm 260) and for the referred thickness were: Plasma arc current 200 A, arc voltage 131 V, cutting speed 2200 mm/min., torch standoff 4.1 mm, O<sub>2</sub> plasma gas flow rate 69 L/min. and shielding gas flow rate 28 L/min. Here, it should be noted that the objective of the research is not to optimize the cutting parameters, but to determine how well-defined industrial parameters affect the cut edge properties and characteristics.

After the cutting process, samples were obtained (from the cut edge area) for metallographic study, hardness measurements and machining of mini-specimens for tensile tests. The metallographic samples were fixed in a conductive acrylic resin (Condufast™, Struers, Cleveland, OH, USA). Then, the surface under observation was polished with SiC papers up to grade 1200 and finally polished with 0.6 µm diamond paste, on velvet, until a specular finish is achieved. The polished samples were etched with 2% Nital for 15 s, rinsed with ethyl alcohol and dried under a hot air stream, before being observed in an optical microscope (Leica MEF-4, Leica, Wetzlar, Germany).

The hardness profiles were made using a LECO hardness tester (model M-400-G2, Leco, Saint Joseph, MI, USA) equipped with a Vickers pyramidal tip. The indentations were carried out with a load of 4.93 N (0.5 kg).

The mini-tensile samples were cut from the plate using a wire electro-discharge machine (WEDM). Four dog bone shaped prisms were cut from the surface of the cut edge, with their longitudinal axes in the direction of the cut. These prisms were in the mid plane of the plate thickness (or the cut edge), as shown in Figure 1.

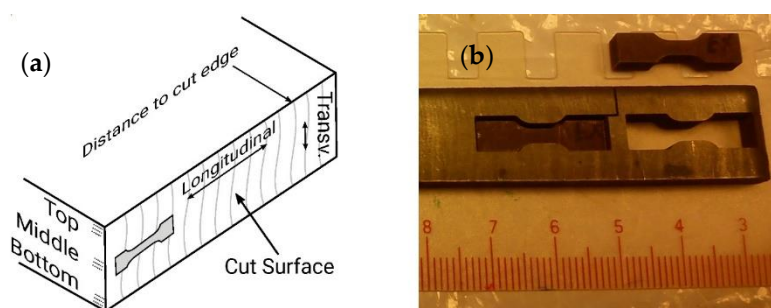


**Figure 1.** (a) General geometry of the cut plate including the orientation of tensile specimens, zones where hardness measurements were made, and directions used for measuring stresses. (b) Extraction of four bone shaped blocks (for later slicing and extraction of the mini-tensile samples), by electro-erosion of the central zone of the cut edge. Scale shown is in millimeters.

These four prisms were sliced into 300  $\mu\text{m}$ -thick specimens. The distance between two consecutive specimens obtained from the same block was also 300  $\mu\text{m}$ , due to the material removed by the wire during the machining process (see Figure 2). In other words, between two consecutive mini-tensile specimens obtained from the same block, there were 300  $\mu\text{m}$  of material that were lost during the machining process that, consequently, could not be characterized. To better characterize the tensile properties all along the depth from the cut edge, the initial cut of each block or prism was moved (in depth) 150  $\mu\text{m}$  from one another. With this shift between blocks, it was possible to obtain mini-tensile samples each of 150  $\mu\text{m}$  in depth (or distance to the cutting edge).



**Figure 2.** Slicing of one of the prisms to obtain tensile mini-samples.

As can be seen from Figures 1 and 2, the mini-tensile samples have a longitudinal orientation (same as the cut edge) and their faces are parallel to the cut edge.

According to the bibliography [17], wire EDM cutting (WEDM) introduces residual stresses up to a depth of approximately 80  $\mu\text{m}$ . To eliminate, as much as possible, the effects of the WEDM, 50  $\mu\text{m}$  were eliminated on each side of the mini-tensile samples by polishing (with SiC grade 1200 sandpaper and a subsequent polishing with 1  $\mu\text{m}$  diamond paste in a velvet cloth) [18]. To remove the material, an automatic Struers polishing machine (Struers, Cleveland, OH, USA) was used. During the polishing, the orientation of the samples was fixed to provide a longitudinal polishing pattern, parallel to the future direction of loading. The final thickness of the mini-tensile samples was nominally 200  $\mu\text{m}$  (the real thickness was measured and recorded for each sample. Average sample thickness was 203  $\mu\text{m}$  with a standard deviation of 25  $\mu\text{m}$ ).

Exceptionally, in the sample containing the surface of the cutting edge, this surface was not removed by polishing, but it was preserved. This first mini-tensile specimen was polished only on the inner side (polishing was carried out removing 100  $\mu\text{m}$  on the inner side, so that the final thickness was also approximately 177  $\mu\text{m}$ ).

Figure 3 shows a mini-tensile sample. Its nominal dimensions are 20 mm in length, 5 mm in total width (the gauge length having 2.5 mm width and 3 mm length) and 0.2 mm in thickness.

To obtain accurate strain measurements, each specimen was instrumented with a strain gauge (HBM 1-LY11-3/120, HBM, Darmstadt, Germany, with 5% maximum strain), as shown in Figure 3. A San-Ei (San-Ei Electric Co., Ltd., Osaka, Japan) amplifier is used to record the lengthening of the strain gauge. The tensile tests were carried out in a universal testing machine with a crosshead displacement speed of 0.1 mm/minute. For deformations greater than 5%, the crosshead position records were used (based on the correlation between the position of the actuator and the previous measurements of the strain gauge). The strain gauge stiffness is not negligible when compared to that of the specimen, and it was measured in an independent test. Thus, the contribution of the strain gauge to the force measured by the load cell was considered when defining the actual load applied to the mini-tensile specimens during tests.

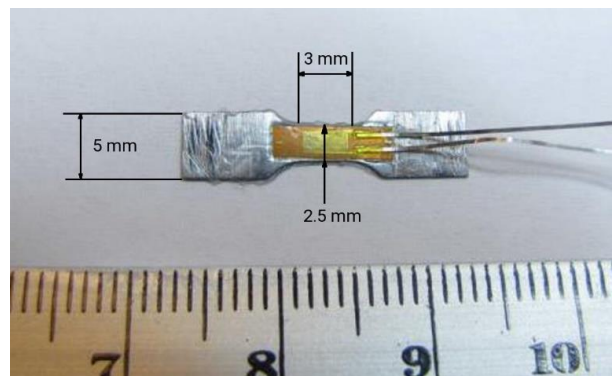


**Figure 3.** Mini-tensile specimen with the strain gauge for measuring deformations up to 5%. Scale shown is in millimeters.

The tensile tests were carried out in an electro-mechanical machine (Instron Mini 44, Instron, High Wycombe, UK). This test machine is equipped with a load cell of  $\pm 500$  N. For fixing the samples, their ends were inserted in two narrow channels machined at the end of two bolts. These channels were  $300 \mu\text{m}$  wide. The mini-tensile samples shoulders were fixed into the channels with a cyanoacrylate adhesive (Loctite); the capillarity of glue guarantees the complete fixation of the sample.

Finally, X-ray diffraction equipment was used to measure longitudinal (along the cutting direction) and transversal (thickness direction) residual stresses at different depths from the cut edge. Prismatic samples of  $8 \times 10 \times 35$  mm were machined (using WEDM) from half the thickness of the plate to avoid the influence of the top/bottom surfaces. These samples were cleaned in a solution of  $500 \text{ mm}^3$  of HCl and  $500 \text{ mm}^3$  of distilled water, for 20 min at room temperature. The measurements were made on a X-Ray diffractometer (X'Pert, Philips, Amsterdam, The Netherlands), with the following parameters: anode material Cr ( $K\alpha_2 = 2.2936663 \text{ \AA}$ ), voltage 40 kV, current 40 mA, angle  $2\theta$  scanning range  $144.1^\circ \sim 166.0^\circ$  ( $0.3^\circ/\text{step}$ ),  $\psi$  scan range  $60.00^\circ \sim 60.00^\circ$  ( $7.76^\circ/\text{step}$ ), time per step 12.05 s. The lattice equivalent planes considered for measuring the residual stresses were the {211}.

For the measurement of stresses at different depths, the cut surface material was eliminated in a controlled manner. To remove these thin layers of steel, an electrolytic polish setup was used. This technique allowed us to remove material without introducing additional stresses in the samples. The material was etched applying a potential of 14 V on blocks in an electrolytic medium made of 90% perchloric acid and 10% ethanol. This procedure (electro-polishing and X-ray diffraction) was repeated four times, until reaching a depth of  $700 \mu\text{m}$  from the original cut surface. The stresses were always measured on the polished surface. The measured residual stress does not correspond to the original stress at that depth because the removal of material induces a relaxation of internal stresses. It is possible to deduce the original stresses at a certain depth,  $\sigma$ , using expression [19]:

$$\sigma(z_1) = \sigma_m(z_1) + 2 \int_{z_1}^H \frac{\sigma_m(z_1)}{z} dz - 6z_1 \int_{z_1}^H \frac{\sigma_m(z_1)}{z^2} dz$$

where  $H$  corresponds to the initial sample thickness,  $z_1$  to the current thickness and  $\sigma_m$  to the measured stress obtained after eliminating the material. An in-house developed code was used to deduce the stress profile that exists on the original plate from measurements and material thickness removed.

To validate this measurement methodology, a set of 5 tests were carried out on a pre-stressed sample. These 5 samples were stressed up to 390 MPa. Results from X-Ray measurements provided stress values of  $388 \pm 7$  MPa.

### 3. Results

#### 3.1. Metallography

Figure 4 shows the metallographic section (already etched) of the zone affected by the cut (CHAZ). In the figure, the left side corresponds to the cut edge, whereas the right side corresponds to the bulk material, or remaining plate. Moreover, the top side of the picture corresponds to the plate surface where the plasma nozzle was located, and the bottom side corresponds to the zone that rested on the cutting table (slag side). Rounding and a thickness reduction of around 1.0 mm are observed in the upper-left zone (jet entry) of the cut. The CHAZ (in principle, the darker material) is very thin, around 0.4 mm deep, especially when compared to that obtained by other cutting procedures with lower energy densities, such as oxyfuel. The latter generates a CHAZ whose depth varies between 1 mm (nozzle side) and 4 mm (slag side) [12,20]. The CHAZ provided by the plasma cut is, however, deeper than that obtained in the same material when cutting with laser, which varies between 0.1 mm (nozzle side) and 0.4 mm (slag side) [12,20]. Moreover, the depth of the CHAZ obtained when performing plasma cuts is nearly constant, whereas oxyfuel and laser cuts generate HAZs with variable depths along the plate thickness.

The heat generated during the cutting process produces phase transformations and the grain growth of the underlying matrix material, as shown in Figure 5. The microstructure shown in this figure corresponds to the area highlighted in the frame in the middle section of Figure 4. Grain size reduces drastically in areas close to the cut edge. At distances from the cut edge greater than approximately 600  $\mu\text{m}$ , there are no changes in grain size.

Just below the cutting edge, layers of martensite and bainite are observed. At a depth of about 200  $\mu\text{m}$  from the cutting edge, polygonal ferrite is observed. At approximately 400–500  $\mu\text{m}$ , the ferrite grains are larger and beyond the 700  $\mu\text{m}$  pearlite and (even larger) polygonal ferrite grains are observed; this last microstructure corresponds to the base material, not affected by the cut (a hypoeutectoid steel, with bands of perlite and ferrite).

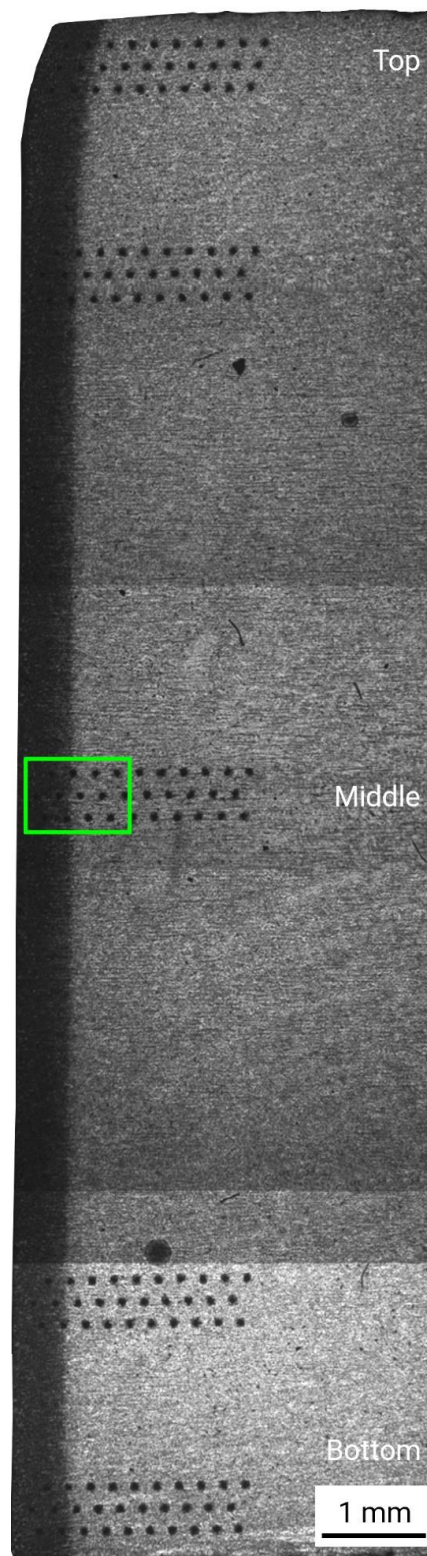
#### 3.2. Microhardness

Figure 6 shows the Vickers hardness profiles (0.5 kg, HV05) of the cutting edge measured at the upper part of the plate (at 0.5 mm and 2.5 mm from the plate upper surface, or nozzle side), at half the thickness plate, and at the lower part of the plate (at 0.5 mm and 2.5 mm from the plate lower surface). The measurements are presented as a function of the distance to the cutting edge (see also Figures 1a and 4 to clarify the position of the measurements). To obtain detailed hardness profiles, indentations of 0.5 kg (4.91 N) were made instead of 1 kg (9.81 N). It is known that non-standard hardness measurements can differ from standard ones but the indentations of half a kilogram are smaller and can be placed closer to one to another and to the cutting edge itself. At each height, three lines of indentations were made, with a small shift between them, with the purpose of obtaining in greater detail the evolution of hardness in the CHAZ versus depth. For each depth a single measurement was made.

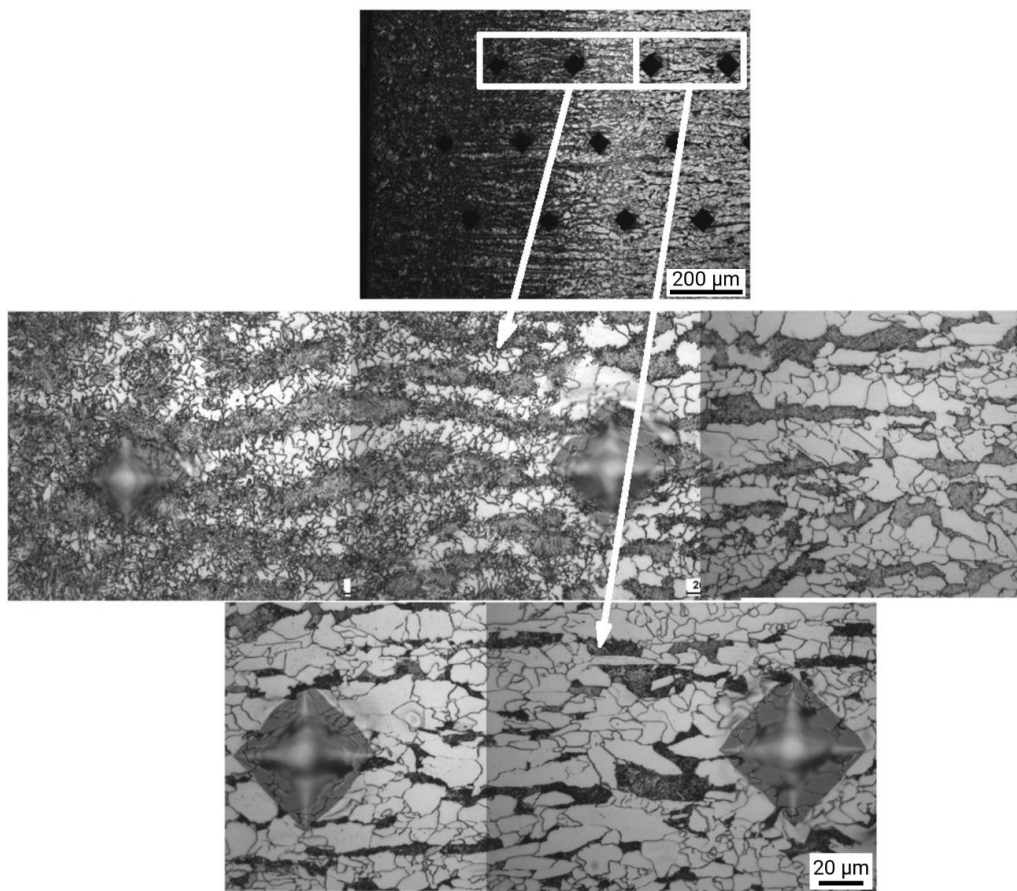
It can be observed that the microhardness measurements provide very similar results in the upper, middle, and lower part of the cut section. This is related with the uniform thickness of the CHAZ, as revealed in the images included in Figure 4. The effect of plasma cutting vanishes at a distance of approximately 700  $\mu\text{m}$  from the cut edge, along all the cut thickness. The European standard EN 1090-2 [21] sets a limit of 380 kg/mm<sup>2</sup> for the Vickers hardness after cutting. The microhardness measured near the surface slightly exceeds this limit in a thin layer, with a depth of about 350  $\mu\text{m}$  (EN 1090-2 [21] specifies Vickers with 1 kg load and here, the results are presented with only 0.5 kg). The problem with a very hard cut surface is that it is prone to cracking in subsequent bending processes. Several bend tests of the cut edges analyzed in the HIPERCUT project were carried out (e.g., [12,22]). All samples tested were bent 180° without cracks, including those specimens that had the entire surface of the cutting edge on the tensile side, revealing that the observed hardness measurements, which are



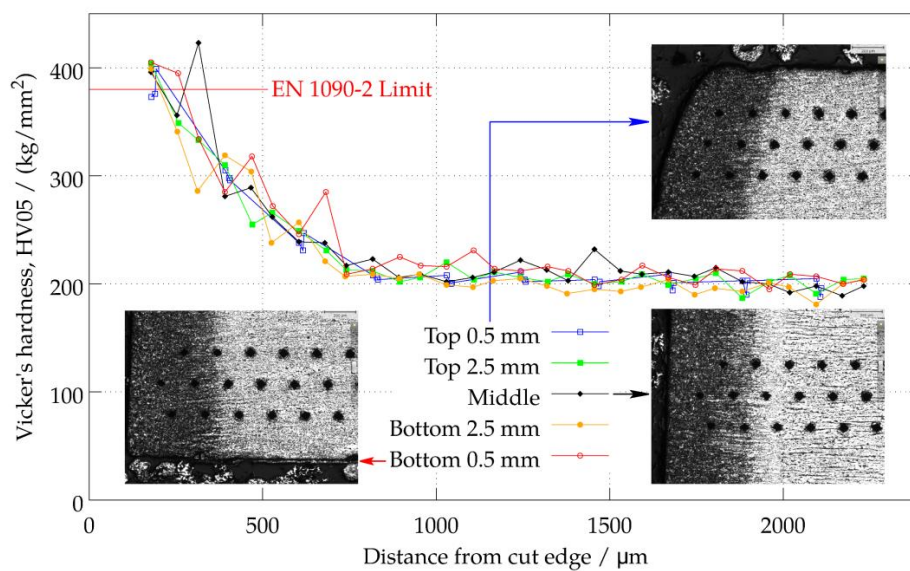
slightly above the limits provided in [21], do not negatively affect the bending behavior of the plasma cut edges analyzed.



**Figure 4.** Optical micrograph of the CHAZ, etched with 2% Nital. The Vickers indentations made for measuring hardness profiles are visible. The upper-left part corresponds to the plasma inlet (see also Figure 1a).



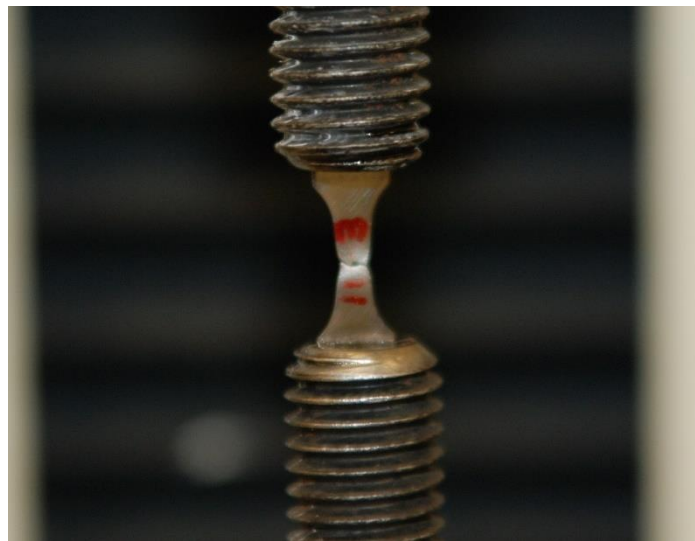
**Figure 5.** Detail corresponding to the framed area on Figure 4 close to the middle section. The microstructures shown in the second row correspond to the zone closer to the cut edge and its microstructure is finer in regions closer to the cut edge (left).



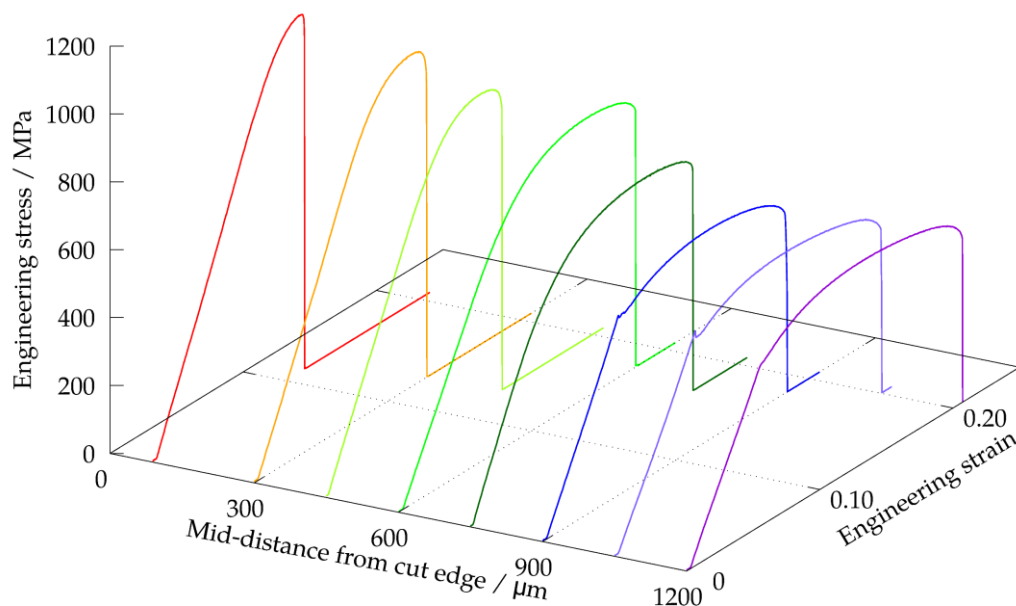
**Figure 6.** Hardness profiles against the distance to the cut edge. Each color corresponds to a region of the sample, blue corresponding to the one closest to the plasma nozzle and red to the region further from the plasma nozzle. Images included in the graph show the microstructure and indentations distribution used to make the plot in three regions (**top**, **middle** and **bottom**).

### 3.3. Mini-Tensile Tests

Figure 7 shows the (ductile) fracture observed in a tensile test, typical of a mini-tensile specimen after necking. Figure 8 summarizes the results obtained in the mini-tensile tests. The engineering stress is plotted against the (engineering) strain, as a function of the distance to the original surface produced by the plasma cut. As mentioned above, the mini-tensile specimens were obtained from four blocks extracted from the center of the thickness of the cut edge. For each depth, a single tensile test was carried out. It can be observed that the closer to the cut edge, the larger the resistance parameters and the lower the ductility. Differences in stress-strain curves tend to stabilize at a distance of approximately 750–900  $\mu\text{m}$ . This is basically consistent with the microhardness measurements made at the center of the cutting edge.



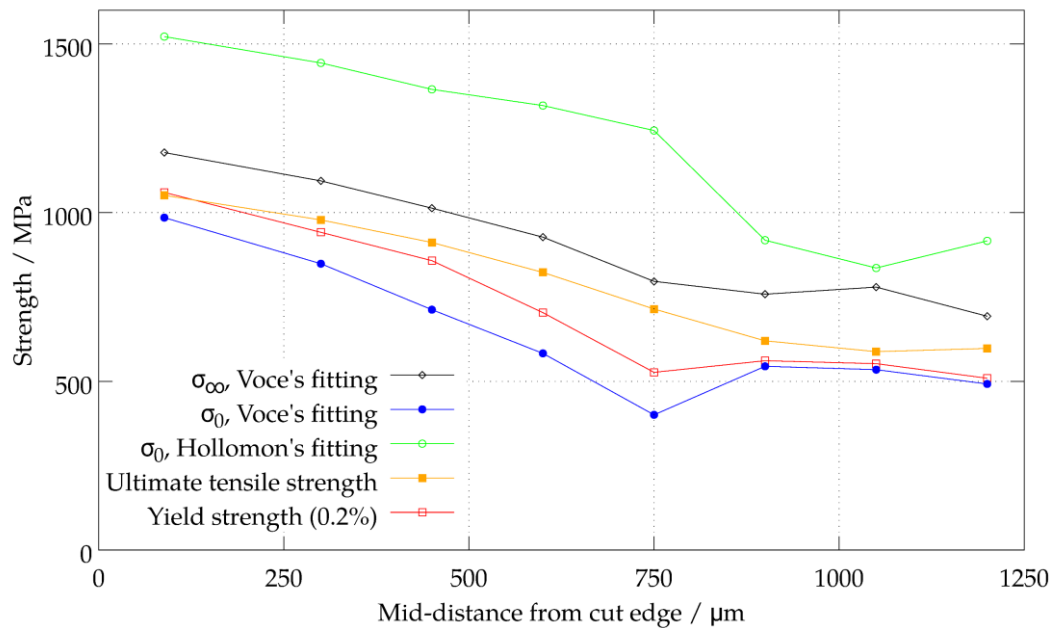
**Figure 7.** Mini-tensile test specimen during tensile test. The top and bottom screws have the channel parallel to the image plane where sample shoulders were glued. The necking and later fracture can be easily observed.



**Figure 8.** Stress-strain curves obtained at different depths from the cut edge.

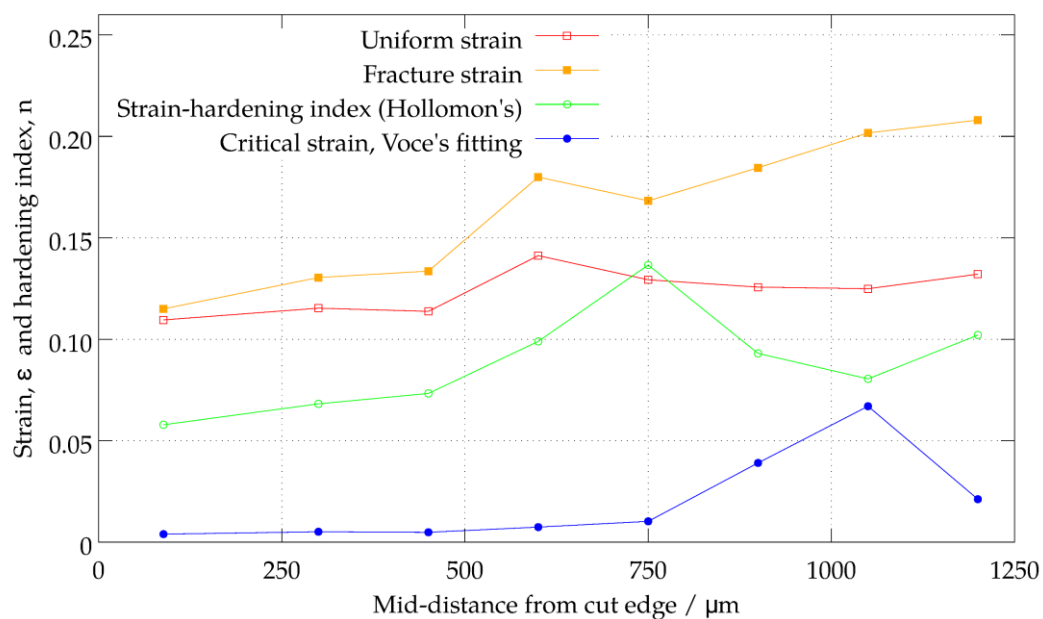


Figure 9 represents the change in the mechanical behavior (yield stress, Ultimate tensile strength, etc.) versus distance to plasma cut, for mini-specimens extracted from the central section of the cut. From this figure, it is clear that the material strength decreases as the distance from cut edge increases. For distances of over 800  $\mu\text{m}$  there are no changes in the ultimate tensile strength, UTS, and the mechanical properties of the base material are reached. Something similar happens with the yield stress, which decreases from 1060 MPa at 88.5  $\mu\text{m}$  to 526 MPa at 750  $\mu\text{m}$ . For distances greater than 750  $\mu\text{m}$  there are no changes in UTS, so it could be assumed that base material has been reached.



**Figure 9.** Evolution of mechanical properties as a function of distance to cut edge.

Figure 10 shows the evolution of the uniform strain (up to necking), fracture strain, hardening index, and critical strain for Voce's fitting, versus distance to plasma cut (Appendix A).



**Figure 10.** Evolution of the uniform strain, fracture strain, hardening index, and critical strain as a function of the distance to edge cut by plasma.

From this figure, it is possible to appreciate that the material gets softer with the distance from the cut edge. There are no significant changes in the ductility over distance but the fracture strain increases, making the material tougher. From the fitting parameters shown in this figure, it is not possible to say that at 1 mm the base material has been reached, but with the information of Figures 8 and 9 it could be assumed that, from a practical point of view, CHAZ reaches 700  $\mu\text{m}$ . This deduced value is smaller than the one observed for other thermal cutting processes [23].

### 3.4. Residual Stresses

Figure 11 shows the residual stresses measured in the longitudinal direction (L) and thickness direction (T) obtained by X-ray diffraction, after its deconvolution. Error in depth was obtained by measuring the removed material in different locations of the sample. The error in residual stress was obtained from the error given by the X-Ray equipment used and the error previously measured in depth. Plasma cutting generates at the surface of the cut a great compression in both directions; L and T (see Figure 1a). The residual compression extends to a distance of approximately 700  $\mu\text{m}$  in the underlying material, located under the cut surface.

The values of these compressive residual stresses measured on the surface are in the order of the material yield stress. These big stresses are probably produced by the great cooling gradients that appear in the plate during the cutting process and they can play a key role in the fatigue behavior of these cut edges (for example, delaying the initiation of cracks and, therefore, increasing fatigue life). However, this behavior also depends on other parameters such as the surface roughness and the microstructural characteristics at those areas underlying the cut [14–17]. Whether or not the removal of the plasma cut surface would be beneficial for the material fatigue performance requires further research.

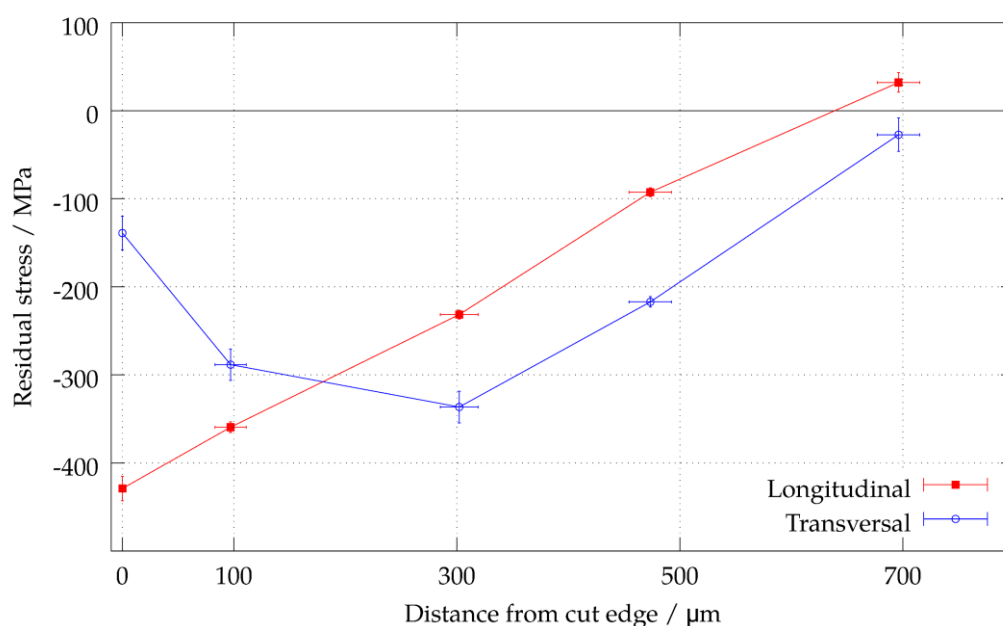


Figure 11. Distribution of residual stresses according to distance to cut edge.

## 4. Conclusions

- The Cut Heat Affected Zone (CHAZ) generated by plasma cutting is quite narrow (around 700  $\mu\text{m}$  and, in any case, lower than 1 mm) and quite uniform across the entire thickness of the cut. These results agree with metallographic observations and microhardness measurements.
- The hardness measured (HV05) on the surface of the cutting edge is slightly higher than the limit set in the standard EN 1090-2 [21] (although it does not seem to affect bend behavior).

- It was possible to obtain Stress-strain curves for the material at different depths under the cut. This was done by testing mini-tensile specimens, extracted by means of WEDM, and instrumented with strain gauges.
- The yield stress and the UTS change with the distance to the cut edge. In the areas closest to the cut, values are obtained that can be 100% higher than those measured at the base material.
- The greater the mechanical strength, the lower the ductility and resilience. Obviously, their values are related to those microstructures formed in the CHAZ.
- Plasma cutting introduces large residual compressive stresses, up to depths of approximately 700  $\mu\text{m}$ .

**Author Contributions:** J.A. wrote the paper, performed the measurements of residual stresses and analyzed X-Ray results. A.M.M. designed mini-tensile tests, prepared the samples, and performed the experiments, analyzing their results. He also contributed with the manuscript. S.C. contributed with the writing of the paper and designed, programmed and analyzed all indentation experiments. A.K. supplied all the samples and performed the bending tests. He also optimized conditions for performing plasma the cuts. A.B. performed the metallography preparation and analysis of the cut samples.

**Acknowledgments:** The authors of this work would like to express their gratitude to the European Union for the financial support of the project HIPERCUT: “High Performance Cut Edges in Structural Steel Plates for Demanding Applications” (RSFR-CT-2012-00027), on the results of which this paper is based.

**Conflicts of Interest:** The authors declare no conflict of interest.

## Appendix A

The simplest fit to tensile behavior (stress vs. strain curve) of a material is given by Hollomon’s expression [24]

$$\sigma = \sigma_0 \varepsilon_p^n \quad (\text{A1})$$

where  $\sigma$  represents the stress as a function of the plastic strain,  $\varepsilon_p$ . Only two parameters are used:  $\sigma_0$  and  $n$ .  $n$  is known as strain hardening index.

A little more sophisticated and realistic is Voce’s relation [25];

$$\sigma = \sigma_\infty - (\sigma_\infty - \sigma_0) e^{-\frac{\varepsilon_p}{\varepsilon_c}} \quad (\text{A2})$$

This expression has three parameters:  $\sigma_\infty$  represents the saturation stress (the stress that ideally will be reached for infinite strain),  $\sigma_0$  is the stress for a negligible plastic deformation and  $\varepsilon_c$  is a critical strain (as shown in Figure A1, at intercept with the abscissa).

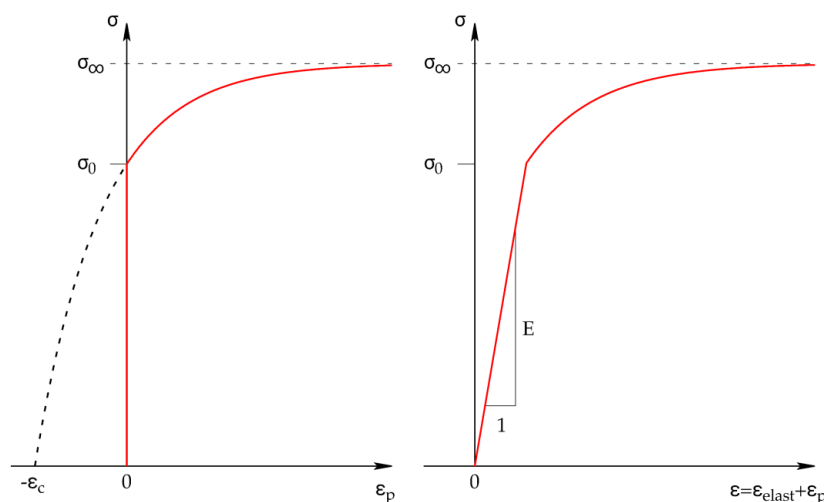


Figure A1. Interpretation of Voce’s parameters.

## References

1. Wood, W.E. *Heat-Affected Zone Studies of Thermally cut Structural Steels (Report FHWA-RD-93-O 15)*; US Department of Transportation Federal Highway Administration: Washington, DC, USA, 1994.
2. Tomas, D.J. Characterisation of Steel Cut Edges for Improved Fatigue Property Data Estimations and Enhanced CAE Durability. Ph.D. Thesis, Swansea University UK, Swansea, UK, 2011.
3. British Standard EN ISO 9013:2002. *Thermal Cutting—Classification of Thermal Cuts—Geometrical Products Specification and Quality Tolerances*; British Standards Institution: London, UK, 2004.
4. Kirkpatrick, I. Variety of cutting processes spoil fabricators for choice. *Weld. Met. Fabr.* **1994**, *62*, 11–12.
5. Avila, M. Which metal-cutting process is best for your application. *Weld. J.* **2012**, *91*, 32–36.
6. The Steel Construction Institute. *Guidance Notes on Best Practice in Steel Bridge Construction*; P185, Fifth Issue; Steel Bridge Group: Ascot, UK, 2010; ISBN 978-1-85942-196-3.
7. EN 1993-1-9: Eurocode 3: Design of Steel Structures—Part 1-9: Fatigue; European Committee for Standardization: Brussels, Belgium, 2005.
8. Goldber, F. Influence of thermal cutting and its quality on the fatigue strength of steel. *Weld. J.* **1973**, *52*, 392–404.
9. Plecki, R.; Yeske, R.; Alstetter, C.; Lawrence, F.V., Jr. Fatigue resistance of oxygen cut steel. *Weld. J.* **1977**, *56*, 225–230.
10. Ho, N.-J.; Lawrence, F.V.; Alstetter, C.J. The fatigue resistance of plasma- and oxygen-cut steel. *Weld. Res.* **1981**, *11*, 231–236.
11. Piraprez, E. *Fatigue Strength of Flame-Cut Plates, Fatigue of Steel and Concrete Structures*; IABSE Reports; International Association for Bridge and Structural Engineering: Zurich, Switzerland, 1982; Volume 37, pp. 23–26.
12. Bannister, A.; Danks, S.; Klimpel, A.; Luksa, K.; Rzeznikiewicz, A.; Cicero, S.; Álvarez, J.A.; García, T.; Martín-Meizoso, A.; Aldazabal, J. *High Performance Cut Edges in Structural Steel Plates for Demanding Applications (HIPERCUT)*; EUR 28092 EN; Directorate-General for Research and Innovation, European Commission: Luxembourg, 2016; ISBN 978-92-79-61684-6.
13. Kaufmann, I.; Schonherr, W.; Sonsino, C.M. Fatigue strength of high-strength fine-grained structural steel in the flame cut condition. *Schweissen u. Schneiden* **1995**, *3*, E46–E51.
14. Cicero, S.; García, T.; Álvarez, J.A.; Martín-Meizoso, A.; Aldazabal, J.; Bannister, A.; Klimpel, A. Definition and validation of Eurocode 3 FAT classes for structural steels containing oxy-fuel, plasma and laser cut holes. *Int. J. Fatigue* **2016**, *87*, 50–58. [[CrossRef](#)]
15. Cicero, S.; García, T.; Álvarez, J.A.; Bannister, A.; Klimpel, A.; Martín-Meizoso, A.; Aldazabal, J. Fatigue behaviour of structural steels with oxy-fuel, plasma and laser cut straight edges. Definition of Eurocode 3 FAT classes. *Eng. Struct.* **2016**, *111*, 152–161. [[CrossRef](#)]
16. Cicero, S.; García, T.; Álvarez, J.A.; Martín-Meizoso, A.; Bannister, A.; Klimpel, A. Definition of BS7608 fatigue classes for structural steels with thermally cut edges. *J. Constr. Steel Res.* **2016**, *120*, 221–231. [[CrossRef](#)]
17. García Navas, V.; Ferreres, I.; Marañón, J.A.; García-Rosales, C.; Gil Sevillano, J. Electro-discharge machining (EDM) versus hard turning and grinding—Comparison of residual stresses and surface integrity generated in AISI O1 tool steel. *J. Mater. Process. Technol.* **2008**, *195*, 186–194. [[CrossRef](#)]
18. Rech, J.; Kermouche, G.; Grzesik, W.; García-Rosales, C.; Khellouki, A.; García-Navas, V. Characterization and modelling of the residual stresses induced by belt finishing on a AISI52100 hardened steel. *J. Mater. Process. Technol.* **2008**, 187–195. [[CrossRef](#)]
19. Moore, G.; Evans, W.P. Mathematical Correction for Stress in Removed Layers in X-ray Diffraction Residual Stress Analysis. *SAE Trans.* **1958**, 340–345. [[CrossRef](#)]
20. Andrés, D.; García, T.; Cicero, S.; Lacalle, R.; Álvarez, J.A.; Martín-Meizoso, A.; Aldazabal, J.; Bannister, A.; Klimpel, A. Characterization of heat affected zones produced by thermal cutting processes by means of Small Punch tests. *Mater. Charact.* **2016**, *119*, 55–64. [[CrossRef](#)]
21. European Standard: EN 1090-2:2011+A1. *Execution of Steel Structures and Aluminium Structures. Part 2: Technical Requirements for Steel Structures*; European Committee for Standardization: Brussels, Belgium, 2011.



22. Klimpel, A.; Cholewa, W.; Bannister, A.; Luksa, K.; Przystalka, P.; Rogala, T.; Skupnik, D.; Cicero, S.; Martín-Meizoso, A. Experimental investigations of the influence of laser beam and plasma arc cutting parameters on edge quality of high-strength low-alloy (HSLA) strips and plates. *Int. J. Adv. Manuf. Technol.* **2017**, *92*, 699–713. [[CrossRef](#)]
23. Martín-Meizoso, A.; Aldazabal, J.; Pedrejón, J.L.; Moreno, S. Resilience and ductility of Oxy-fuel HAZ cut. *Frattura ed Integrità Strutturale* **2014**, *30*, 14–22. [[CrossRef](#)]
24. Hollomon, J.H. Tensile deformation. *Trans. AIME* **1945**, *162*, 268–277.
25. Voce, E. The Relationship between Stress and Strain for Homogeneous Deformation. *J. Inst. Met.* **1948**, *74*, 537–562.



© 2018 by the authors. Licensee MDPI, Basel, Switzerland. This article is an open access article distributed under the terms and conditions of the Creative Commons Attribution (CC BY) license (<http://creativecommons.org/licenses/by/4.0/>).